EUV-induced carbon growth at contaminant pressures between 10^{-10} mbar and 10^{-6} mbar: Experiment and model

S.B. Hill, C. Tarrio, R.F. Berg, T.B. Lucatorto

Sensor Science Division

National Institute of Standards and Technology

Gaithersburg, MD 20899-8411 USA

Carbon contamination induced by ultraviolet (UV) radiation affects precision optics in applications as diverse as semiconductor lithography and satellite observations of the Sun. Our previous experiments have shown that low-intensity UV-induced surface contamination depends quasi-logarithmically on the partial pressure of the organic contaminant due to the poly-dispersive nature of the surface-adsorbate system. This complex dependence presents difficulties because, without a physically motivated model, it cannot be extrapolated to low pressures. We present measurements and a model of carbon growth induced by UV exposure in the presence of tetradecane vapor. The model, which includes a coverage-dependent adsorption energy, describes the measurements over four orders of magnitude in pressure, and we expect that it can be extrapolated to the lower pressures of interest to the extreme ultraviolet (EUV) lithography and solar astronomy communities. Our experience with other contaminants leads us to expect that other organic contaminants will behave similar to tetradecane. The results also provide insights into the kinetics governing coverage isotherms at extremely low partial pressures.

I. Introduction

Carbon deposition on optics due to the cracking of organics in the presence of short-wavelength radiation has been recognized since at least 1910.[1] In recent years this carbon contamination has become an increasing concern for EUV lithography[2,3] and long-term solar monitoring.[4] Energetic photons interact with adsorbed organic molecules, either directly or via emitted secondary electrons, and break bonds, reducing the volatility of the molecules. Eventually a permanent carbonaceous layer grows. At UV to EUV wavelengths, where all materials are absorbing, carbon greatly reduces the reflectance or transmittance of any optical system. In an EUV lithography scanner, approximately ten mirrors are used to reflect and focus 13.5 nm radiation onto the photoresist.[5] This means that deposition of only 1 nm of carbon contamination creates a 10% loss of throughput, which can reduce the number of wafers printed per hour below the point of economic viability. Similarly, in the monitoring of the EUV solar irradiance for climate models, the data interpretation must account for the thickness and absorption spectrum of any carbon that is deposited during the years-long lifetime of the satellite. This increases the uncertainty of the total solar irradiance and its time evolution, and it necessitates frequent recalibrations made by comparing the satellite instruments to recently calibrated instruments flying on sounding rockets.

We have studied the carbon-growth process by irradiating samples with EUV radiation in the presence of organic contaminants.[6,7,8] To mimic the long-term exposure effects observed in a reasonable time, these experiments used elevated pressures, generally in the range of 10^{-9} mbar to 10^{-6} mbar, which is orders of magnitude higher than the partial pressures of contaminants in EUV lithography or satellite systems. Tying these accelerated experiments to real-life situations requires a model that can be extrapolated with confidence to lower pressures. We believe that

the model described here can do so. Our confidence is supported by measurements of carbon grown using EUV radiation in the presence of *n*-tetradecane over four orders of magnitude in partial pressure.

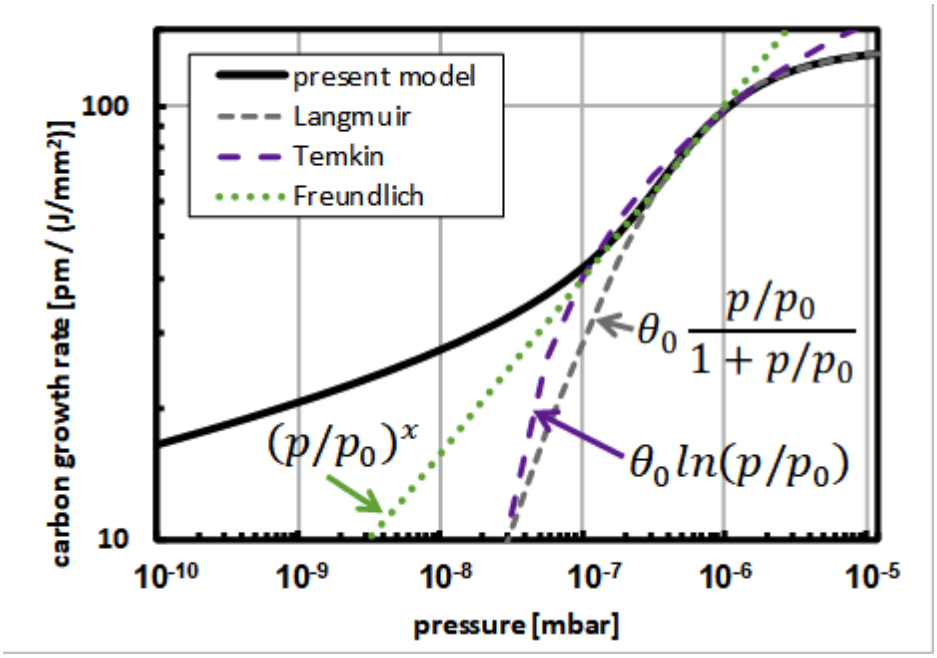

Figure 1. Unlike the present model, some frequently used isotherms can underpredict the carbon growth at low pressures. The quantities θ_0, p_0, and x for those isotherms were fit to data within the range from 1.2×10^{-7} mbar to 1.2×10^{-6} mbar.

In the low-intensity regime far from intensity saturation, the carbon growth rate is proportional to the amount of carbon available from molecules adsorbed on the surface, which is in turn determined by the equilibrium between thermal desorption and molecular impingements. The two models most commonly used to describe the equilibrium dynamics and the resulting surface coverage are the Langmuir[9] and Temkin[10] models and resulting isotherms. See Fig. 1. The Langmuir model assumes a constant adsorption energy for a given molecule, and it leads to a coverage that is approximately linear in pressure over limited pressure ranges. The Temkin

model assumes an adsorption energy that also includes a term that is proportional to coverage to account for site competition. This leads to a coverage that depends on the logarithm of the pressure over limited ranges. Our earlier work with several volatile organics at pressures below 10^{-4} mbar demonstrated that the coverage in those situations more closely approximates the Temkin model over limited ranges of pressure. The current model is an improvement that allows extrapolation to low pressures.

II. EUV-induced carbon growth rates measured in admitted gas experiments.

EUV exposures were carried out at Beamline 8 (ref. 11) of the NIST Synchrotron Ultraviolet Radiation Facility,[12] shown schematically in Figure 2. Briefly, radiation from SURF is collected and focused by a spherical multilayer mirror operating at 10° angle of incidence and coated to reflect 13.4 nm radiation. A thin-film Be filter captured in the gate of a gate valve[13] provides rejection of long-wavelength radiation and also serves as a vacuum barrier preventing the upstreaming of introduced gases. The combination of SURF irradiance, mirror reflectivity, and filter transmission lead to a spectrum peaked at 13.2 nm with a full-width at half-maximum of 0.5 nm. The environmental chamber has a manifold of leak valves that allow the introduction of controlled partial pressures of a variety of gases. The chamber is turbo-pumped and has a base pressure of 5×10^{-9} mbar dominated by H_2 and H_2O. The partial pressures of organic species above a mass to charge ratio of 45 are all $<<10^{-12}$ mbar. Samples are introduced through a load lock that has an atomic hydrogen cleaning system to remove adventitious organic material from the sample surface. We chose both Ru-capped Mo/Si trilayer samples, which simulate the top layers of multilayer mirrors used in EUVL, and Au-coated Si wafer tokens as the samples.

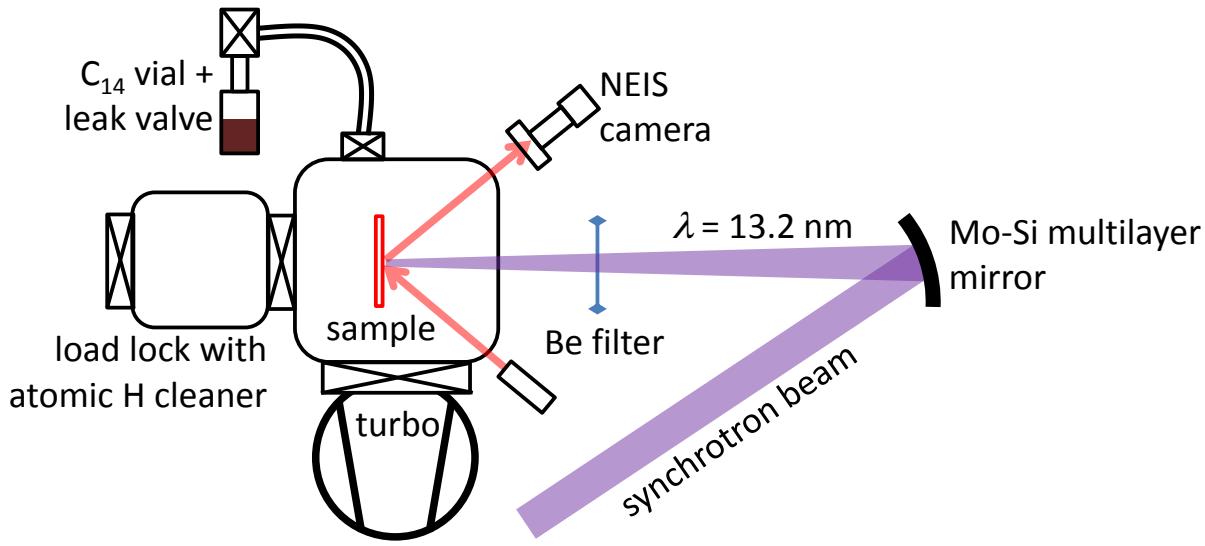

Figure 2. Schematic of the end station on SURF beamline 8.

Carbon growth was monitored in real time with a null-field imaging ellipsometer (NEIS)[14] and an electrometer that measured the photoemission current. The electrometer was connected between the sample and ground. A bias of 200 V was applied to an extraction electrode located 2 cm from the sample surface. These two *in-situ* determinations were calibrated approximately by *ex-situ* thickness measurements. The *in-situ* estimates had sufficient accuracy that the endpoint of an exposure could be chosen to achieve a peak target carbon thickness to within ± 0.3 nm.

The partial pressure of the volatile organics was determined from the total pressure measurement of a cold cathode gauge (CCG) above 10^{-8} mbar, well above the background levels of water and H_2. Below 10^{-8} mbar the m/e=57 amu/e peak of a residual gas analyzer (RGA) was used to determine the tetradecane partial pressure independent of the background species. To obtain absolute partial pressures, the CCG was calibrated against a spinning rotor gauge over their common ranges of 10^{-6} mbar to 10^{-5} mbar. This calibration was then transferred to the RGA

by correlating it with the CCG over their common ranges of 10^{-8} mbar to 10^{-7} mbar. We estimate the standard relative uncertainty of the partial pressures reported here as 5 % above 10^{-8} mbar, and 17 % below 10^{-8} mbar.

X-ray photoelectron spectroscopy (XPS) was used to measure the thickness of the grown carbon. The XPS measurements used an Al K_α monochromatic source with a spot size of about 0.2 mm. This resolution was sufficient to measure the distribution of the deposited C spot in detail with a raster map (typically 15 by 15 with 0.25 mm spacing). The associated EUV spot had a well-quantified quasi-Gaussian intensity distribution, which allowed us to obtain a range of thicknesses as a function of dose from a single C spot.

The carbon thickness was obtained by measuring the attenuation of the substrate peak area by the overlayer of carbon.[15] On the Ru-coated samples the Ru $3p_{3/2}$ peak was measured to avoid problems due to the overlap of the C 1s and Ru 3d peaks, and an effective attenuation length (EAL) of λ_{Ru3p} = 2.1 nm was assumed based on previous measurements of graphitic C.[16]

For the Au-coated samples, the Au $4f_{7/2}$ peak was measured, and λ_{Au4f} = 2.7 nm was determined by scaling λ_{Ru3p} by the ratio of EALs for the Au and Ru peaks given by the predictive formula of Seah.[17]

Figure 3 shows the results of these low-intensity measurements on *n*-tetradecane on the two substrates. The dependence on the partial pressure of *n*-tetradecane differs from both the quasi-linear behavior of the Langmuir model and the quasi-logarithmic dependence of the Temkin model. Our earlier measurements on isobutene, benzene, toluene, and tert-butylbenzene showed similar behavior.[18] We also see that the two data sets are independent of the substrate surface material. This is expected because these data were taken after roughly 1.5 nm (about 5 monolayers) of C had been deposited, and thus represent a C-on-C growth rate.

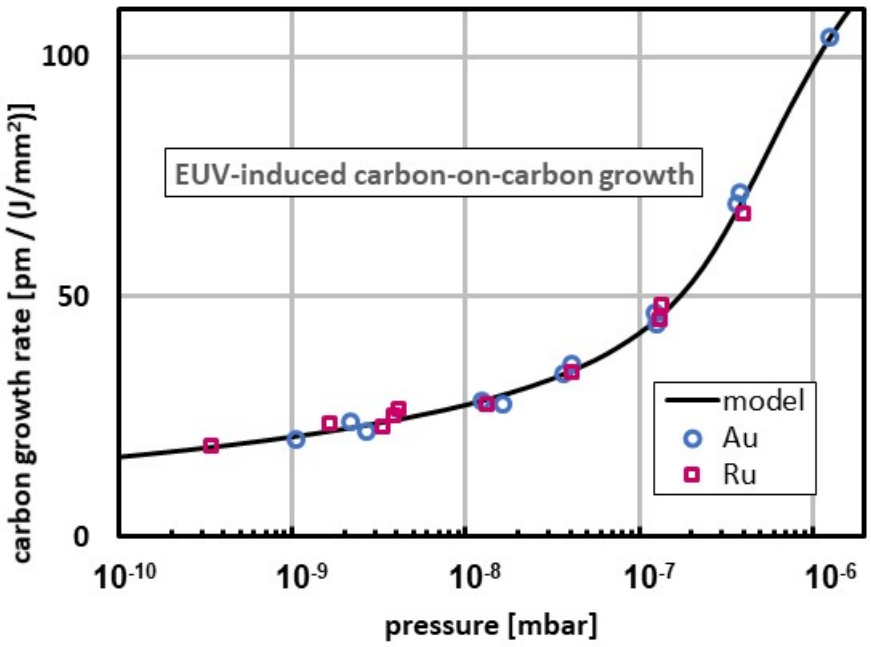

Figure 3. Carbon-on-carbon growth measured at multiple tetradecane partial pressures, exposure times, and EUV intensities.

III. The kinetics governing coverage: Detailed balance between EUV-induced dissociation, desorption, and molecular impingement.

The steady-state contamination rate is the result of a balance between four competing processes: the photon-activated cracking of the adsorbed organic contaminant; photon-stimulated desorption of the adsorbate; thermal desorption of the adsorbate; and replenishment of the adsorbate from molecular impingement. At low intensities thermal desorption dominates the photon-activated processes, and the carbon contamination rate depends linearly on the intensity and the coverage. At higher intensities, where the photon-activated processes dominate the thermal desorption, an intensity saturated regime is observed where the contamination rate is determined by the molecular impingement rate. Our studies were done in the low-intensity

regime since we are most interested in the equilibrium coverages that are not significantly affected by the photon flux.

Our model of carbon growth, which is similar to previous models,[19,20] assumes the following:

- We are in the low-intensity regime, where the carbon growth rate is proportional to the EUV intensity I (photon s^{-1} m^{-2}).
- The growth occurs irreversibly. Desorption, dissociation, and chemical bonding occur only in the top layer of adsorbed tetradecane, while no change occurs in the lower layers of deposited carbon.

With these assumptions, the total thickness D of the carbon increases at the rate

(1) $$\frac{dD}{dt} = \tau I \sigma_c N_{C/R} \theta (n_M/n_C) .$$

Here σ_c is the cross section that characterizes the cracking and chemical bonding of an adsorbed molecule, whether caused by the direct absorption of a photon or by its secondary electrons, and $N_{C/R}$ is the resulting average number of carbon atoms that are bonded to the surface per event. Also, τ is the thickness of a monolayer of carbon, $0 < \theta < 1$ is the coverage of adsorbed tetradecane molecules, n_M is the number of tetradecane molecules per unit area in one monolayer, and n_C is the number of carbon atoms per unit area in a monolayer. The unknown ratio n_M/n_C is between approximately 1/14 and 1, corresponding respectively to molecules that lie parallel and perpendicular to the substrate. If measured by the unit dose, $q = I\, t\, E_{ph}$, with E_{ph} the photon energy, Eq. (1) becomes:

(2) $$\frac{dD}{dq} = \frac{\theta N_0 \sigma_c \tau}{E_{ph}}$$

with $N_0 = N_{C/R}\,(n_M/n_C)$.

The coverage θ is determined by an equilibrium between thermal desorption, molecular impingement, and UV-induced dissociation. The thermal desorption rate, $r(\theta,T)$, for first-order processes is well represented by the Polanyi-Wigner formula:[21]

$$r(\theta,T) = \theta n_M \nu \exp\left(\frac{-E(\theta)}{kT}\right), \quad (3)$$

where ν is a frequency prefactor, and $E(\theta)$ is an effective adsorption energy for the molecular species on the surface.

In general, both $E(\theta)$ and ν depend on the substrate, the adsorbate, and the coverage θ. We inferred the value of ν from measurements made elsewhere, specifically measurements of temperature-programmed desorption (TPD) of *n*-alkanes on graphite,[22,23] MgO,[24,25] and Pt and C.[26] In TPD, a clean sample is exposed to a controlled dose of the molecule of interest, then heated at a constant rate. During the heating, a mass spectrometer monitors the desorbed flux, and a curve of the desorption rate as a function of temperature is obtained. Analysis of TPD data relies on the Polanyi-Wigner formula, Eq. (3).

Paserba and Gellman[22,23] measured the TPD spectra of 21 *n*-alkanes (C_5 to C_{60}) on graphite while using heating rates from 0.1 K s^{-1} to 5 K s^{-1}. Varying the heating rate allowed them to obtain independent values of $E(\theta)$ and ν. Notable results included:

- The value of the frequency prefactor ν was roughly independent of the alkane chain length, and its value, about 10^{19} s^{-1}, was much larger than the nominal value kT/h = 6×10^{12} s^{-1}, where k is the Boltzmann constant and h is the Planck constant.
- The desorption energy had a nonlinear dependence on chain length that could be modeled by considering both the energy and the entropy of the alkane interacting with the substrate.[27]

- The desorption energy E was weakly dependent on the coverage θ. Their modeling of the desorption energy as

(4) $$E(\theta) = E_0 + E_1\theta$$

yielded E_1/E_0 close to 0 for n-alkanes with fewer than 16 carbons and less than 0.05 for chains up to 40 carbon atoms. The ratio E_1/E_0 is a measure of the importance of adsorbate-adsorbate interactions.

Tait, et al.,[24,25,26] obtained independent TPD values of $E(\theta)$ and ν for n-alkanes with 10 or fewer carbon atoms. In Ref. 26 they described the coverage dependence of $E(\theta)$ by:

(5) $$E(\theta) = E_0 + E_1\theta + E_d e^{-\theta/\theta_d} .$$

The energy E_d is the difference between the energies of the most tightly bound (first to populate) sites and the average sites of the substrate. For a crystal substrate, E_d can be thought of as the extra adsorption energy of a defect and θ_d as the fraction that characterizes the density of defects. Their values for $E(\theta)$ at $\theta = 0.5$ agree well with those of Paserba and Gellman, but there is some discrepancy in the values of $E_1(\theta)$ and ν. Figure 4 compares the results of the two studies' determinations of ν. Paserba and Gellman find a fairly constant value of about 10^{19} s^{-1}, while Tait et al. find an increase with chain length. The two studies intersect at a chain length of about 14 carbons, and we elected to fix ν at 10^{19} s^{-1} at that intersection point.

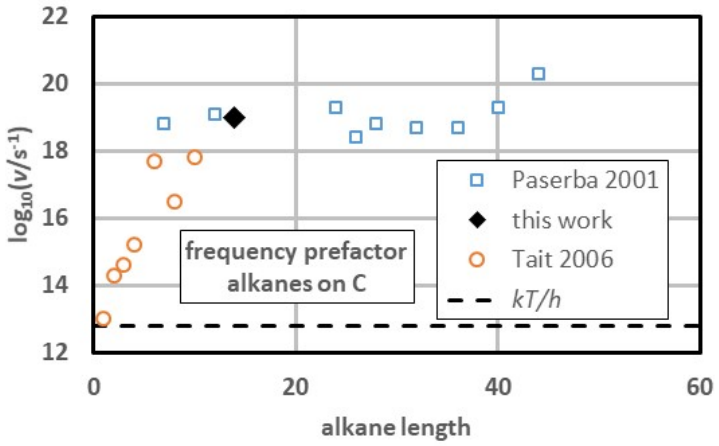

Figure 4. Values of the frequency prefactor ν measured in Refs. 23 and 25 for n-alkanes on graphite. The value in this work was defined to be 10^{19} s^{-1}.

Detailed balance in steady state implies that the impingement of molecules onto a surface equals the sum of thermal desorption, photo-desorption, and UV-induced dissociation. Assuming that the sticking coefficient for impinging molecules is 0 for occupied adsorption sites and 1 for unoccupied sites, the steady-state coverage is given by:

(6) $$(1-\theta)\Phi = \theta n_M \nu e^{-\frac{E(\theta)}{kT}} + \theta n_M I \sigma_T \, .$$

Here, Φ is the impingement rate given by:

(7) $$\Phi = \frac{p}{\sqrt{2\pi m k T}} ,$$

where p is the partial pressure of the contaminant, m is the mass of the molecule, and $\sigma_T = \sigma_d + \sigma_c$ is the total photon cross section for events that make an intact adsorbed molecule unavailable, whether by desorption (σ_d) or by cracking and bonding to the surface (σ_c). Rearranging Eq. (6) gives:

(8) $$\theta = \frac{\Phi}{\Phi + n_M \nu e^{\frac{-E(\theta)}{kT}} + n_M I \sigma_T} ,$$

which shows that an adsorption energy $E(\theta)$ that increases with decreasing coverage leads to a coverage that decreases sub-linearly with pressure, as is observed in the Temkin-like isotherms and in this work.

IV. Modelling the carbon on carbon growth.

Substituting Eq. (8) into Eq. (2) gives the equation that we used to describe the results in Fig. 2, where $E(\theta)$was determined by the best fit as described below:

(9) $$\frac{dD}{dq} = \frac{\Phi N_0 \sigma_c \tau / E_{ph}}{\Phi + n_M \nu e^{-\frac{E(\theta)}{kT}} + n_M I \sigma_c},$$

As has been done elsewhere[20,28], the denominator of Eq. (9) neglects EUV-induced desorption by making the approximation $\sigma_T \approx \sigma_c$. This simplification removes the desorption cross section σ_d as a free parameter. We note that Zalkind et al. [29], who exposed TiO_2 surfaces simultaneously to benzene and 100 eV electrons, found that $\sigma_T \approx 3\sigma_c$, which meant that more of the adsorbate was removed by desorption than by carbonization. Fortunately, this approximation caused no problem because the present results were obtained at low intensity, so that the term $n_M \sigma_c I$ never exceeded 2 % of the denominator of Eq. (9).

Figure 1 demonstrates that neither the Langmuir isotherm model, which assumes a constant value for $E(\theta)$, nor the Temkin isotherm model, which assumes a linear increase in energy with coverage, i.e., $E(\theta) = E_0 + E_1\theta$ as described by Paserba and Gellman[23], represent the actual measurements over an extended range. Instead the best fit was provided by the form for $E(\theta)$ suggested by Eq. (5) of Tait et al.[25], with $E_1 = 0$, a value consistent with the findings of Paserba and Gellman[23] and Tait et al.[25] for chain lengths smaller than 20 carbons.

Guided by the measurement of 2.2×10^{18} m^{-2} for the monolayer surface density n_M of benzene on Pt,[30] we assume $n_M = 10^{18}$ m^{-2} for tetradecane on the surfaces of our samples. After also assuming the value $\nu \equiv 10^{19}$ s^{-1}, Eq. (9) is left with five free parameters: the adsorption energy parameters E_0, E_d, and θ_d, the cross section σ_c, and the number N_0, which is of order unity. Although the values assumed for ν and n_M have significant uncertainty, they have only a small effect on the fitted values. For example, increasing ν or n_M by a factor 3 can be compensated by increasing E_0 by 2%. The choice of the multiplying factor N_0 is unimportant for intensities I where the growth rate is proportional to I and thus the factor $n_M I \sigma_c$ in the denominator is negligible. At these low intensities the choice of N_0 has only a small effect on E_0. We assumed $N_0 = 1$.

Thus, the parameters E_0, E_d, θ_d, and σ_c for C-on-C growth were obtained by fitting the data to Eq. (9). In practice, the fitting procedure was applied iteratively to all the carbonization data until the deviations between the model and the data were minimized for all the EUV exposure conditions -- 21 separate cases for the Ru-capped trilayers and 24 cases for the Au films. Figure 3 shows the data for C-on-C growth for all of the measured cases along with the model prediction based on the parameters in Table 1.

Table 1. Parameter values used to describe carbon-on-carbon growth.

monolayer thickness	τ	0.27	nm	ref [20]
density of C_{14} molecules in a full monolayer	n_M	1×10^{18}	m^{-2}	defined
thermal desorption, frequency prefactor	ν	1×10^{19}	s^{-1}	defined
thermal desorption, typical adsorption energy	E_0	110.5	kJ mol^{-1}	fit
thermal desorption, C_{14}-C_{14} interaction	E_1	0	kJ mol^{-1}	defined
thermal desorption, defect energy	E_d	73.0	kJ mol^{-1}	fit
thermal desorption, defect fraction	θ_d	0.0788		fit
carbonization cross section (assuming N_0=1)	σ_c	7×10^{-24}	m^2 $molecule^{-1}$	fit

V. Discussion

The exponential term, $E_d \exp(-\theta/\theta_d)$, suggested by Tait et al.[25] to account for a limited number of defects with higher adsorption energy, seems well justified on physical grounds, and in our case it allows a good fit over four orders of magnitude in pressure. We believe that the behavior similar to that of *n*-tetradecane that we have observed in several other volatile organic adsorbates[18] will obey the same functional dependence.

Our fitted values for E_0, E_d, and σ_c compare favorably to values obtained elsewhere for similar systems. Our value of E_0 = 110.5 kJ mol^{-1} is close to the values of 118 kJ/mol extrapolated from analyses Tait *et al.* and 128 kJ/mol found by Paserba and Gellman, as shown in Fig. 5. Our value for σ_c was $7.4\text{x}10^{-24}$ m^2. Assuming the main EUV process was dissociation by the secondary electrons, we can use our measured photoyield of 0.010 ± 0.005 electrons/photon to estimate an electron-impact dissociation cross-section 7.4×10^{-22} m^2. A

cross-section for adsorbed tetradecane has not been measured; however, a cross-section of 4.5×10^{-22} m^2 has been measured for 20 eV electrons on physisorbed hexane,[31] indicating that our result is physically reasonable.

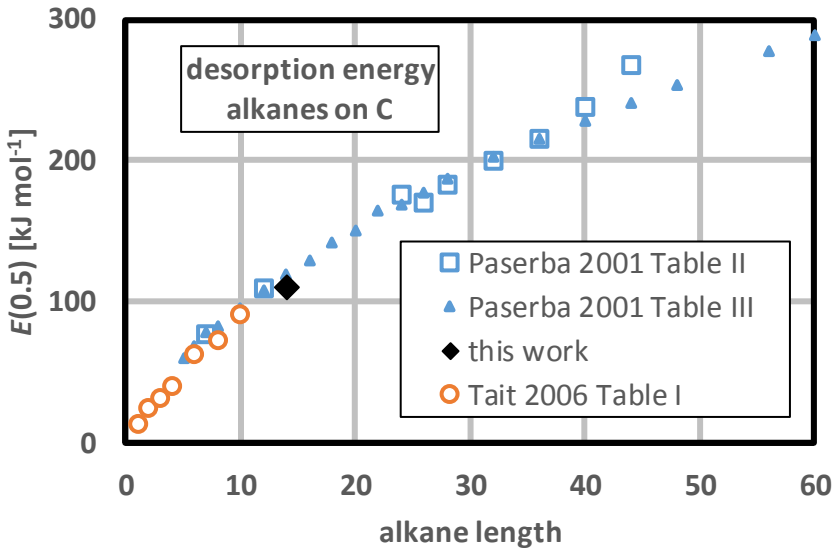

Figure 5. Values measured elsewhere of the desorption energies for n-alkanes on graphite and MgO. The value in this work was determined by fitting Eq. (9) to the carbonization data.

Most of the present measurements were made in the low-light limit far from intensity saturation. This non-saturated region occurs where the thermal desorption rate is much larger than the photon-stimulated removal of the adsorbed molecule or:

(10) $$I\sigma \ll \upsilon e^{-\frac{E(\theta)}{kT}}.$$

Since $E(\theta)$ increases as p and therefore θ decreases, we expect that for an attainable intensity the inequality of Eq. (10) will be reversed as the contaminant pressure is lowered. Figure 6 illustrates this by using Eq. (9) for the three radiation intensities of 0 mW mm^{-2}, 1 mW mm^{-2}, and

10 mW mm^{-2}. At 10^{-10} mbar the coverage at zero intensity is more than an order of magnitude higher than at higher intensity. Note that the "low-intensity" measurements in Figure 3 were measured at irradiances between 0.5 mW mm^{-2} and 5 mW mm^{-2}. At the lowest pressures measured, that range was just below the transition between linear and saturated growth shown in Figure 6.

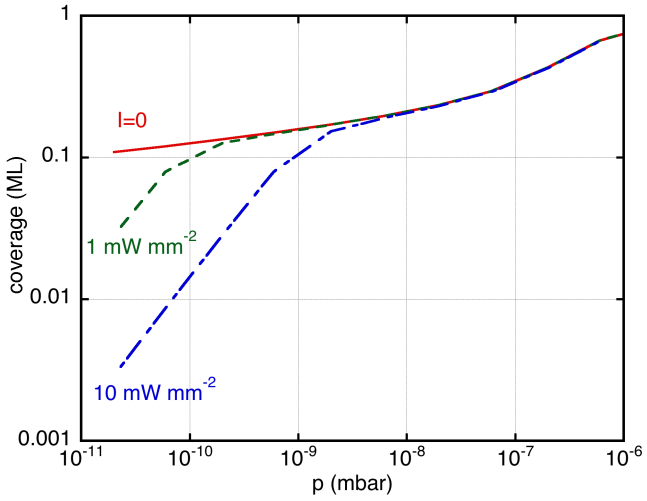

Figure 6. Calculated coverages with no incident light (solid line), 1 mW mm^{-2} and 10 mW mm^{-2}. The deviations below 10^{-8} mbar occur because photon-stimulated removal of the adsorbed molecules becomes comparable to thermal desorption.

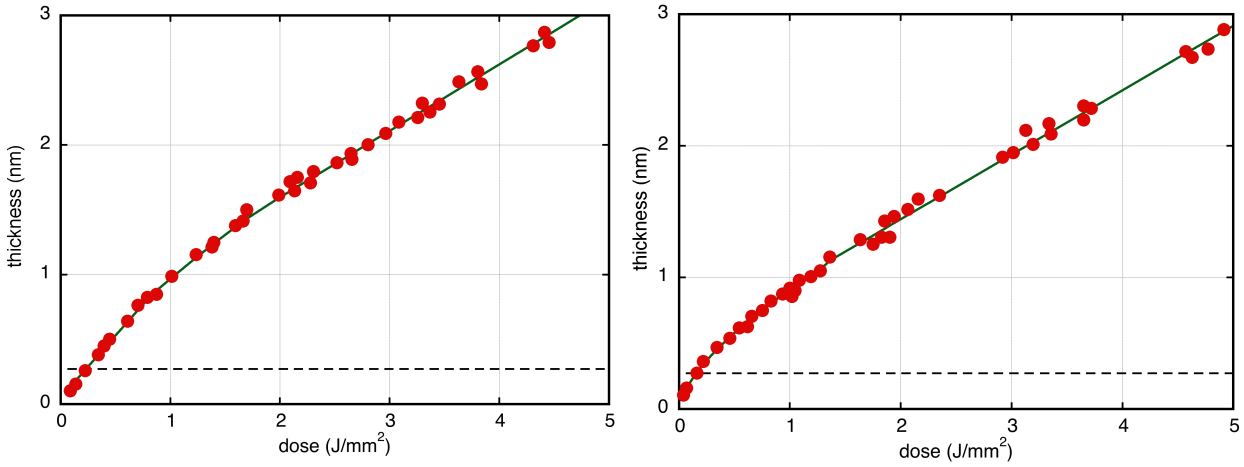

Figure 7. Examples of the growth of carbon on a Ru/Si/Mo trilayer substrate (left) and on a Au-on-Si substrate (right). The solid horizontal lines indicate the thickness of one monolayer of C, and the solid curves are an empirical two-layer model.

The carbon growth modeled in Figure 3 is that of carbon on carbon, which is independent of the base substrate once the carbon thickness exceeds several monolayers. However, even sub-monolayer coverage on mirror surfaces is important because it can significantly degrade an EUV lithographic system. Figure 7 shows the thickness measured as a function of dose on examples of the two substrates. The C-on-C rates plotted in Figure 3 are the slopes of curves such as these in the linear portion, i.e. for thicknesses > 1.5 nm.

The initial slopes in Figure 7 are clearly higher. To describe the entire growth curve, we created a two-layer model that empirically describes the transitions of the adsorption energies and the photoyields from growth on metal to growth on C. For both substrates, the effective adsorption energy should change from the metal value to the C value after the deposition of the first monolayer, around 0.3 nm. The effective photoyield, however, should transition exponentially over a longer distance corresponding to the scattering length of <5 eV electrons,

around 1 nm [17]. We expect the photoyield transition to be more important for the Au samples because the photoyield measured for the bare Au substrate was at least 3 times larger than for the Ru substrate; this is consistent with the more gradual transition of the Au substrate.

It was not possible to extract reliable values for the photoyields and adsorption energies of the metal substrates due to the limited data available for thicknesses < 1 nm. Nevertheless, the different transitions of the Ru and Au substrates show that both parameters are important.

VI. Conclusions

Guided by measurements of EUV-induced carbon growth at multiple tetradecane pressures, exposure times, and EUV intensities, we developed a model that accurately describes carbon growth over four orders of magnitude in pressure. At partial pressures below 10^{-7} Torr, the growth of carbon was higher than expected from isotherms for ideal surfaces (Langmuir) or adsorbate-adsorbate interactions (Temkin), and a single desorption energy for an ideal surface was inadequate to describe our results. Rather, the data down to 3×10^{-10} mbar were explained quite well by an empirical coverage-dependent desorption energy based on a distribution of adsorption sites more representative of a real surface. Values for thermal desorption energy and electron-impact cross-section derived from our model agree favorably with previously published values.

VII. Acknowledgments

We wish to thank the late Ted Madey as well as Lee Richter and Bruce Kay for many helpful discussions.

References

[1] D. Berthelot and H. Gaudenchon, "The chemical effects of ultraviolet rays on gaseous bodies -- the effects of polymerisation," *Comptes Rendus Hebdomadaires des Seances de l'Academie des Sciences* **150**, 1169-1172 (1910).

[2] M. Totzeck, W. Ulrich, A. Goehnermeier, and W. Kaiser, "Semiconductor fabrication -- pushing deep ultraviolet lithography to its limits," *Nature Photonics* **1**, 629-631 (2010).

[3] "Optics Contamination," C. Tarrio, S. B. Hill, R. F. Berg, and S. Bajt, Chapter 6A in *EUV Lithography, Second Edition,* edited by Vivek Bakshi, SPIE Press, Bellingham, WA, 335-367 (2018).

[4] A. BenMoussa et al., "On-orbit degradation of solar instruments," *Solar Phys.* **288**, 288-389 (2013).

[5] henke.lbl.gov/optical_constants/ .

[6] M. Malinowski, C, Steinhaus, M. Clift, L. E. Klebanoff, S. Mrowka, and R. Soufli, "Controlling contamination in Mo/Si multilayers by Si surface-capping modifications," *Proc. SPIE* **4688**, 442-453 (2002).

[7] B. Mertens et al., "Progress in EUV optics lifetime expectations," *Microelectronic Engineering* **73-74**, 16-22 (2004).

[8] C. Tarrio and S. Grantham, "A synchrotron beamline for extreme-ultraviolet multilayer mirror testing," *Rev. Sci. Instrum.* **76**, 046105 (2005).

[9] I. Langmuir, "The adsorption of gases on plane surfaces of glass, mica, and platinum," *J. Am. Chem. Sci.* **40**, 1361-1403 (1918).

[10] M. I. Temkin and V. Pyzhov, "Recent modifications to Langmuir isotherms," *Acta Physicochimica U.R.S.S.* **12**, 217-222 (1940).

[11] S. B. Hill, I. Ermanoski, S. Grantham, C. Tarrio, T. B. Lucatorto, T. E. Madey, S. Bajt, M. Chandhok, P. Yan, O.Wood, S.Wurm, and N. V. Edwards, "EUV testing of multilayer mirrors: critical issues," *Proc. SPIE* **6151**, 61510F-1 (2006).

[12] U. Arp, C. Clark, L. Deng, N. Faradzhev, A. Farrell, M. Furst, S. Grantham, E. Hagley, S. Hill, T. Lucatorto, P.-S. Shaw, C. Tarrio and R. Vest, "SURF III: A flexible synchrotron radiation source for radiometry and research," *Nucl. Inst. Meth. A* **649**, 12-14 (2011).

[13] C. Tarrio and S. Grantham, "A synchrotron beamline for extreme-ultraviolet multilayer mirror endurance testing," *Rev. Sci. Instrum.* **76**, 056101-104 (2005).

[14] R. Garg, N. Faradzhev, S. Hill, L. Richter, P. S. Shaw, R. Vest, and T. B. Lucatorto, "A simple null-field ellipsometric imaging system (NEIS) for *in-situ* monitoring of EUV-induced deposition on EUV optics," Proc. SPIE vol. 7636, *Extreme Ultraviolet Lithography*, edited by B. M. La Fontaine, 76361Z (2010).

[15] S.Hofmann, in *Practical Surface Analysis*, edited by D.Briggs and M. P. Seah, John Wiley, Chichester, p. 168 (1983).

[16] B. Lesiak, A. Jablonski, Z. Prussak, P. Mrozek, "Determination of the Inelastic Mean Free Path of Electrons in Solids," *Surf. Sci.* **223**, 213-232 (1989).

[17] M. P. Seah, "Simple universal curve for the energy-dependent electron attenuation length for all materials," *Surf. Interface Anal.* **44**, 1353–1359 (2012).

[18] S. B. Hill, N. S. Faradzhev, L. J. Richter, and T. B. Lucatorto, "Complex species and pressure dependence of intensity scaling laws for contamination rates of EUV optics determined by XPS and ellipsometry," *Proc. SPIE* **7376**, 73760E (2010).

[19] K. Boller, R-P. Haelbich, H. Hogrefe, W. Jark, and C. Kunz, "Investigation of carbon contamination of mirror surfaces exposed to Synchrotron Radiation," *Nucl. Inst. Meth.* **208**, 273-279 (1983).

[20] J. Hollenshead and L. Klebanoff, "Modeling radiation-induced carbon contamination of extreme ultraviolet optics," *J. Vac. Sci. Tech. B* **24**, 64-82 (2006).

[21] M. Polanyi and E. Wigner, "The breeding and breakdown of molecules," *Z. Phys.* **33**, 429-434 (1925).

[22] K. R. Paserba and A. J. Gellman, "Kinetics and energetics of oligomer desorption from surfaces," *Phys. Rev. Lett.* **86**, 4338-4341 (2001).

[23] K. R. Paserba and A. J. Gellman, "Effects of conformational isomerism on the desorption kinetics of n-alkanes from graphite," *J. Chem. Phys.* **115**, 6737-6751 (2001).

[24] S. L. Tait, Z. Dohnalek, C. T. Campbell, and B. D. Kay, "n-alkanes on MgO(100). I. Coverage-dependent desorption kinetics of n-butane," *J. Chem. Phys.* **122**, 164707 (2005).

[25] S. L. Tait, Z. Dohnalek, C. T. Campbell, and B. D. Kay, "n-alkanes on MgO(100). II. Chain-length dependence of kinetic desorption parameters for small n-alkanes," *J. Chem. Phys.* **122**, 164708 (2005).

[26] S. L. Tait, Z. Dohnalek, C. T. Campbell, and B. D. Kay, "n-alkanes on Pt(111) and on C(0001)/Pt(111): Chain-length dependence of kinetic desorption parameters," *J. Chem. Phys.* **125**, 234308 (2006).

[27] A. J. Gellman and K. R. Paserba, "Kinetics and mechanism of oligomer desorption from surfaces: n-alkanes on graphite," *J. Phys. Chem. B* **106**, 13231-13241 (2002).

[28] V. Jindal, R. Garg, G. Denbeaux, and A. Wüest, "Assumptions and trade-offs of extreme ultraviolet optics", *Alternative Lithographic Technologies*, edited by Frank M. Schellenberg, Bruno M. La Fontaine, Proc. of SPIE Vol. **7271**, 72713Q (2009).

[29] S. Zalkind, B.V. Yakshinskiy, and T.E. Madey, "Interaction of benzene with TiO2 surfaces: Relevance to contamination of extreme ultraviolet lithography mirror capping layers", *J. Vac. Sci. Tech. B* **26**, 2241 (2008).

[30] J. L. Gland and G. A. Somorjai, "Low-energy electron diffraction and work function studies of benzene, naphalene, and pyridine adsorbed on Pt(111) and Pt(100) single-crystal surfaces," *Surf. Sci.* **38**, 157-186 (1973).

[31] G. Leclerc, Z. Cui, and L. Sanche, "Effective dissociation cross-section for the low-energy (0.5-31 eV) electron-impact on solid n-hexane films," *J. Phys. Chem.* **91**, 6461-6463 (1987).